CMS Physics Analysis Summary

Contact: cms-pag-conveners-susy@cern.ch 2019/03/21

Combined search for gauge-mediated supersymmetry with photons in 13 TeV collisions at the CMS experiment

The CMS Collaboration

Abstract

A combination of searches for signatures with at least one photon motivated by generalized models of gauge-mediated supersymmetry breaking is presented. All searches make use of proton-proton collision data at $\sqrt{s} = 13$ TeV recorded by the CMS detector at the LHC. The results of four analyses targeting separate experimental signatures incorporating an isolated photon and significant missing transverse energy are combined. These signatures include events with two isolated photons, events with single leptons that accompany the photon, and events with additional jets. Based on the 35.9 fb^{-1} of integrated luminosity collected in 2016, this combination probes the allowed parameter space of General Gauge Mediation and exceeds the sensitivity of the individual searches to supersymmetric particles by up to 100 GeV in mass.

1 Introduction

The search for supersymmetry (SUSY), a favored theoretical extension of the standard model (SM) of particle physics, is a central piece of the physics program at the CERN LHC. SUSY provides several explanations for unsolved problems in particle physics, including a mechanism for stabilizing the SM-like Higgs boson mass at the electroweak (EWK) energy scale. Supersymmetric models utilizing a general gauge-mediated (GGM) breaking mechanism [1–6] and R-parity conservation [7] often lead to final states containing photons and a significant transverse momentum imbalance [8–15]. These signatures are probed by several searches based on the data set collected by the CMS experiment in 2016 [16–19].

The results of the combined search are interpreted in a GGM signal scenario with photons in the final state scanning the bino and wino mass parameters. In order to provide more model independent results for similar signal topologies the results of the combination are also interpreted in the context of simplified model scenarios (SMS) [20]. These models, based on both electroweak and strong production, allow for a scan of the gaugino branching fractions resulting in final states with photons.

In this note, a combination of four different searches focusing on GGM SUSY scenarios is presented. In GGM SUSY, the gravitino ($\widetilde{\mathrm{G}}$) is the lightest SUSY particle (LSP) and escapes undetected, leading to an observed missing transverse momentum ($p_{\mathrm{T}}^{\mathrm{miss}}$). The lightest neutralino ($\widetilde{\chi}_1^0$) corresponds to the next-to-lightest SUSY particle (NLSP), which decays, depending on its composition, to a photon (γ), a Z boson, or a Higgs boson (H), and a $\widetilde{\mathrm{G}}$. Additional SM particles can arise from the decay of the lightest chargino ($\widetilde{\chi}_1^{\pm}$) and, in the case of strongly produced SUSY particles, from gluino and squark decays.

All searches used in the combination are performed with proton-proton (pp) collision data at a center-of-mass energy $\sqrt{s} = 13$ TeV corresponding to an integrated luminosity of $35.9\,\mathrm{fb}^{-1}$, collected with the CMS detector in 2016. Each search defines a category of events used in the combination which all contain isolated photons and large missing transverse momentum. The first category requires the presence of two isolated photons (Diphoton category). This category is based on the search presented in [19] and targets bino-like neutralino decays leading to final states with two photons. Charged leptons are vetoed in this event category. The second category requires one isolated photon as well as one isolated charged lepton (Photon+Lepton category). For the charged leptons (e, μ), in the following simply referred to as leptons, the selection requirements correspond to the veto in the Diphoton category mentioned above, avoiding overlap between the two categories. This category is based on the search presented in [18]. The third category requires the presence of at least one isolated photon and significant missing transverse momentum utilizing the variable $S_T^{\gamma} = p_{\mathrm{T}}^{\mathrm{miss}} + \sum_{\gamma_i} p_T(\gamma_i)$ (Photon+S_T^{γ} category). No explicit requirement on other objects is imposed in this category. The category is based on the search presented in [17] and provides sensitivity to both electroweak and strong production of SUSY particles with at least one photon in the final state. The fourth category requires at least one isolated photon and significant hadronic activity by selecting events with a high values of the variable $H_T^{\gamma} = H_{\mathrm{T}} + p_T^{\gamma}$, where H_{T} is the scalar sum of the transverse momenta of all jets in the event (Photon+H_T^{γ} category). The category is based on the search presented in [16] and focuses on SUSY scenarios based on strongly produced gluinos and squarks with at least one photon in the final state.

The overlap of the four categories is removed in an optimized way to maximize the sensitivity of the combination. Compared to the individual searches the combination extends the sensi-

tivity to GGM SUSY in both electroweak and strong production scenarios and yields the first consistent set of CMS results across SUSY searches in events with photons at $\sqrt{s} = 13$ TeV.

The note is organized as follows. The signal scenarios considered for the interpretation are described in Section 2. A brief description of the CMS detector is given in Section 3, followed by the description of the object reconstruction and identification in Section 4. Section 5 outlines the event selection and categorization that combines the four categories. In Section 6 the results of the combination are presented and summarized in Section 7.

2 Signal Scenarios

For the GGM scenario considered, the squark and gluino masses are set to a high scale rendering them irrelevant to the studied LHC collisions, such that strong production is negligible and electroweak production of gauginos is dominant. The GGM framwework used to derive the GGM scenario is suitable for unifying general models of gauge-mediation in a model-independent way [21–23]. For the GGM scenario, also referred to as M1M2 scenario, the techniques in [23] are used to reduce the 8-dimensional GGM parameter space to two gaugino mass parameters. The M1M2 scenario is defined by setting the GGM parameters as follows:

$$M_3 = \mu = 8 \text{ TeV} \tag{1}$$
$$m_Q = m_U = 10 \text{ TeV} \tag{2}$$
$$m_D = 8 \text{ TeV} \tag{3}$$

The parameters M_3 and μ are the gluino and higgsino mass parameter, respectively, and the parameters m_Q, m_U, and m_D are the sfermion soft masses. This allows to scan over the remaining bino (M_1) and wino (M_2) mass parameters. All parameters are defined at the messenger scale, which is set to $M_{mess} = 10^{15}$ GeV.

Both models satisfiy the Higgs mass constraint. In pure GGM, the lifetime of the NLSP is a function of the NLSP and the gravitino mass. In order to ensure prompt decays of the NLSP on detector scales, the gravitino mass is fixed at 10 eV. Alternatively, the gravitino mass could be kept light by lowering M_{mess}. In [22] it was shown that this would imply heavy squarks ($m_{\tilde{q}} \gtrsim 3$ TeV), which is consistent with the scans performed in this work. Due to the heavy squarks and gluinos both scenarios are dominated by EWK production involving $\widetilde{\chi}_1^{\pm}\widetilde{\chi}_1^{\mp}$, $\widetilde{\chi}_1^{\pm}\widetilde{\chi}_1^{0}$, and $\widetilde{\chi}_1^{\pm}\widetilde{\chi}_2^{0}$ production. One possible diagram for the GGM scenario is shown in Fig. 1 (upper left). The branching fraction (BF) of the NLSP decaying into a photon and a gravitino is determined by the composition of the gauge eigenstates of the NLSP. As shown in Fig. 2 (left), the BF of the NLSP changes across the M1M2 parameter space. For large M_1 and medium M_2 the NLSP is wino-like increasing the probability for $\widetilde{\chi}_1^0 \to \mathrm{Z}\widetilde{\mathrm{G}}$ decays in the case where the NLSP mass exceeds m_Z. The NLSP mass exceeds the Z boson mass if $M_2 \gtrsim 300$ GeV. For the remaining phase space the NLSP is bino-like. The different compositions of the NLSP can also be extracted from the dependence of the physical NLSP mass on the model parameters M1 and M2, as shown in Fig. 2 (right). While for a wino-like NLSP the physical mass scales with M2, for the remaining phase space with bino-like NLSPs the physical mass depends on M1. For the whole phase space the physical NLSP mass range is of the order of 100 to 700 GeV.

Based on EWK SMS two different BF scenarios are constructed. In case of the Neutralino BF scenario, $\widetilde{\chi}_1^{\pm}\widetilde{\chi}_1^{0}$ and $\widetilde{\chi}_1^{\pm}\widetilde{\chi}_1^{\mp}$ production are probed, as shown in Fig. 1 (upper right). The chargino is assumed to decay to the NLSP and low-momentum (soft) particles outside the acceptance, while the probabilities for the decay modes $\widetilde{\chi}_1^0 \to \gamma\widetilde{\mathrm{G}}$ and $\widetilde{\chi}_1^0 \to \mathrm{Z}\widetilde{\mathrm{G}}$ are scanned. For the

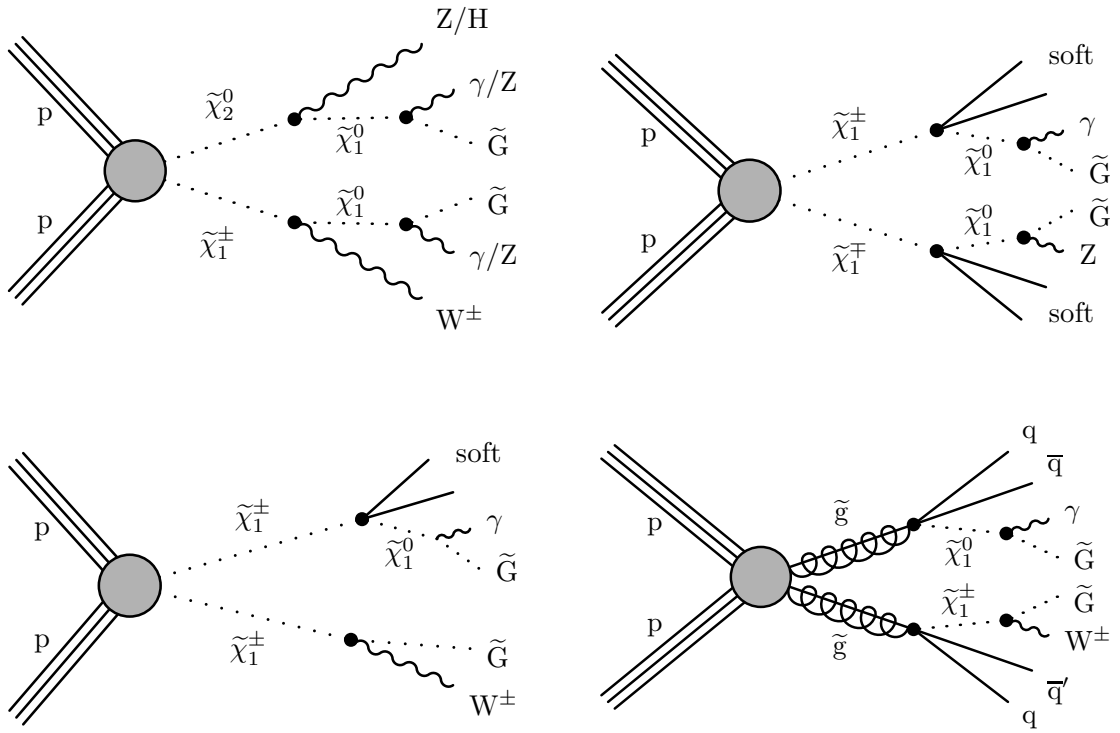

Figure 1: In the GGM scenarios several production and decay channels are possible. The diagram of one possible process based on $\widetilde{\chi}_1^{\pm}\widetilde{\chi}_2^0$ production is shown (upper left), where the gaugino decays depend on the corresponding composition of the gauge eigenstates. In the Neutralino BF scenario $\widetilde{\chi}_1^{\pm}\widetilde{\chi}_1^{\mp}$ (upper right) and $\widetilde{\chi}_1^{\pm}\widetilde{\chi}_1^0$ production are probed. The Chargino BF scenario (lower left) probes $\widetilde{\chi}_1^{\pm}\widetilde{\chi}_1^{\mp}$ production. In the lower right diagram gluino pair production is shown including the charged and uncharged gluino decay.

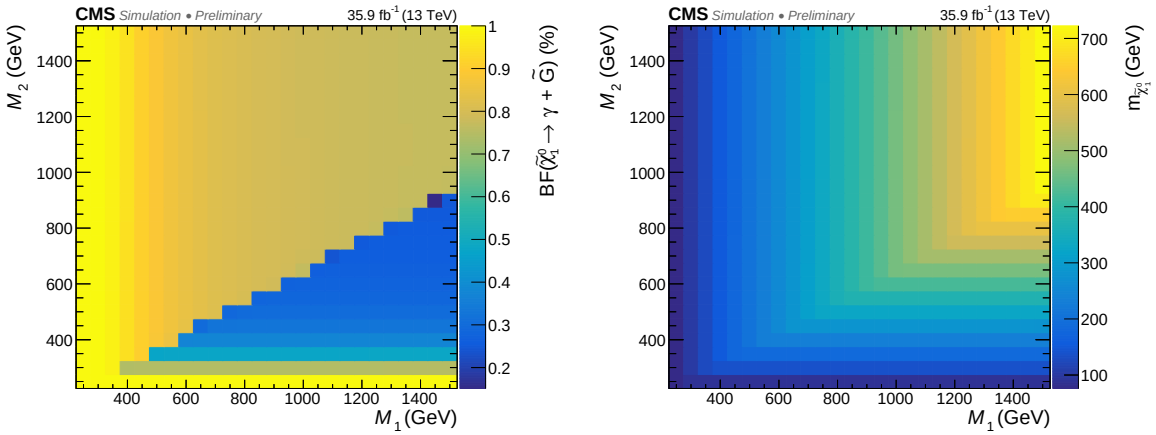

Figure 2: Branching fractions for the NLSP decay to a photon and a gravitino for the M1M2 scenario (left). The phase space is spanned by the bino and wino mass parameters and a change of the NLSP composition is visible. The change of the NLSP composition also influences the dependence of the physical mass of the neutralino on the gauge mass parameters (right).

Chargino BF scenario, shown in Fig. 1 (lower left), only $\widetilde{\chi}_1^{\pm}\widetilde{\chi}_1^{\mp}$ production is probed scanning the probabilities for the decay modes $\widetilde{\chi}_1^{\pm} \to \mathrm{W}^{\pm}\widetilde{\mathrm{G}}$ and $\widetilde{\chi}_1^{\pm} \to \widetilde{\chi}_1^0(+\text{soft})$.

The strong production SMS, shown in Fig. 1 (lower right), is used as nominal Gluino scenario,

as well as to construct the Gluino BF scenario. In both scenarios gluino pair production is probed, assuming charged and neutral decays of the gluino. While the BF for the charged and neutral gluino decay is equally set to 50% in the nominal Gluino scenario, these BFs are scanned in the case of the Gluino BF scenario with the gluino mass set to 1950 GeV. The decay modes for the neutralino and chargino are fixed to $\widetilde{\chi}_1^0 \to \gamma\widetilde{\mathrm{G}}$ and $\widetilde{\chi}_1^{\pm} \to \mathrm{W}^{\pm}\widetilde{\mathrm{G}}$, respectively.

The production cross sections for all points considered in the GGM scenarios are computed at NLO using the PROSPINO 2 framework [24]. The uncertainties on the cross section calculation are derived with PROSPINO to make use of PDFs in the LHAPDF data format [25] following the PDF4LHC recommendations [26]. The simulation used the NNPDF 3.0 [27] parton distribution functions set and was interfaced to Pythia8 [28] using the CUETP8M1 generator tune to describe parton showering and the hadronization [29]. The simplified model signals are generated with MADGRAPH5_aMC@NLO at LO. The cross sections for these models are calculated at NLO and NLO+NLL accuracy [30–38]. All generated events are processed with a fast simulation of the CMS detector response [39].

3 The CMS Detector

The central feature of the CMS apparatus is a superconducting solenoid of 6 m internal diameter, providing a magnetic field of 3.8 T. Within the solenoid volume are a silicon pixel and strip tracker, a lead tungstate crystal electromagnetic calorimeter (ECAL), and a brass and scintillator hadron calorimeter (HCAL), each composed of a barrel and two endcap sections. Forward calorimeters extend the pseudorapidity coverage provided by the barrel and endcap detectors. Muons are detected in gas-ionization chambers embedded in the steel flux-return yoke outside the solenoid.

In the barrel section of the ECAL, an energy resolution of about 1% is achieved for unconverted or late-converting photons in the tens of GeV energy range. The remaining barrel photons have a resolution of about 1.3% up to a pseudorapidity of $|\eta| = 1$, rising to about 2.5% at $|\eta| = 1.4$. In the endcaps, the resolution of unconverted or late-converting photons is about 2.5%, while the remaining endcap photons have a resolution between 3 and 4% [40].

A more detailed description of the CMS detector, together with a definition of the coordinate system used and the relevant kinematic variables, can be found in Ref. [41].

4 Object Reconstruction and Identification

Photons, electrons, muons, and jets are reconstructed with the particle-flow (PF) event algorithm [42], which reconstructs particles produced in a collision combining information from all detector subsystems. The energy of photons is directly obtained from the ECAL measurement. Likewise, electrons are formed from a combination of the momentum measured in the tracker and the energy measured from spatially-compatible clusters of energy deposits in the ECAL. Muons are reconstructed based on the tracks that can be spatially associated to measurements in the muon chambers. Charged and neutral hadrons are also reconstructed by associated tracks with ECAL and HCAL energy deposits. Jets are reconstructed from PF candidates with the anti-kT clustering algorithm [43] with a distance parameter of 0.4.

The missing transverse momentum vector $\vec{p}_{\mathrm{T}}^{\,\mathrm{miss}}$ is computed as the negative vector sum of the transverse momenta of all the PF candidates in an event, and its magnitude is denoted as $p_{\mathrm{T}}^{\mathrm{miss}}$ [44]. The $\vec{p}_{\mathrm{T}}^{\,\mathrm{miss}}$ is modified to account for corrections to the energy scale of the reconstructed jets in the event.

Photons considered in this note are required to be isolated and have an ECAL shower shape consistent with a single photon shower. The diphoton category uses medium-purity photon identification criteria to surpress backgrounds from QCD multijet events [19]. The other three categories use the same loose identification criteria [16–18] to preserve a high signal efficiency. Due to a higher energy resolution of photons reconstructed in barrel region of the CMS ECAL compared to the endcap regions, only photons reconstructed in the barrel region are used.

Reconstructed jets are used to compute the H_T^γ variable along with the selected photons. To prevent double counting of the energy sum, jets within a cone of $\Delta R = \sqrt{(\Delta\phi)^2 + (\Delta\eta)^2} < 0.4$ of the lead photon are not considered in the H_T^γ variable. Jets with $p_\mathrm{T} > 30$ GeV and $|\eta| < 3.0$ are used.

Electrons and muons are selected with the identification criteria described in [19] using the mini-isolation described in [45].

5 Event Selection

Events are divided into the four categories shown in Table 1. Each category is based on one of the four individual searches [16–19]. The minimum photon p_T is mainly determined by the trigger requirements in each of the four searches. Selected diphoton events are binned in $p_\mathrm{T}^\mathrm{miss}$, while events with a photon and a lepton are binned in p_T^γ, H_T, and $p_\mathrm{T}^\mathrm{miss}$. For the Photon+$S_T^\gamma$ and Photon+H_T^γ categories, also referred to as inclusive categories in the following, S_T^γ and $p_\mathrm{T}^\mathrm{miss}$ combined with H_T^γ are used to bin the signal region, respectively.

To enable a statistical combination of the four categories, the overlap between the categories is removed by applying additional vetoes. Since the Diphoton and Photon+Lepton category show the largest sensitivities for both GGM scenarios, these categories remain unchanged with respect to the initial searches. Events with leptons or two photons that are selected in the other two categories, but also match the requirements of the Diphoton or Photon+Lepton category, are vetoed in the Photon+S_T^γ and Photon+H_T^γ category. To remove the overlap between the two inclusive categories the two categories are separated as follows. Events with a large hadronic activity ($H_T^\gamma > 2$ TeV) are vetoed from the Photon+S_T^γ category if they match the $p_\mathrm{T}^\mathrm{miss}$ requirement of the Photon+H_T^γ category. In addition, events with lower hadronic activity ($H_T^\gamma < 2$ TeV) are vetoed from the Photon+H_T^γ category and assigned to Photon+S_T^γ. This preserves the sensitivity of the Photon+H_T^γ category to strongly produced SUSY events as well as the sensitivity of the Photon+S_T^γ category to electroweakly produced SUSY scenarios.

The observed yields as well as the background predictions for the Photon+S_T^γ and Photon+H_T^γ category, which slightly differ from the yields in the initial searches [16, 17] due to the additional vetoes, are shown in Table 2. The yields for the two remaining categories, which are not affected by additional vetoes, can be found in [18, 19].

6 Results

Figure 3 shows the comparison between the data and the background prediction for the search bins used in the combination. In case of the Photon+Lepton and Diphoton categories the comparisons correspond to the published results. The yields of the Photon+S_T^γ and Photon+H_T^γ categories are based on the modified event selections, which ensure exclusive signal regions. For most of the 49 search bins good agreement between the observed events and the background prediction is found, with few bins of the Photon+H_T^γ, Photon+Lepton, and Diphoton

Table 1: Exclusive definitions of the four categories. The kinematic cuts and the search bins are based on the four initial searches. The additional vetoes ensure exclusive event categories. Diphoton and Lepton veto match the event selection described in [19] and [18].

Diphoton Category		
Kinematic Cuts	Search Bins (GeV)	Vetoed Events
$p_{\mathrm{T}}^{\gamma} > 40$ GeV, $p_{\mathrm{T}}^{\mathrm{miss}} > 100$ GeV $m_{\gamma\gamma} > 105$ GeV, Lepton Veto for $p_{\mathrm{T}}^{\ell} > 25$ GeV	$p_{\mathrm{T}}^{\mathrm{miss}}$: [100, 115], [115,130],[130,150] [150,185],[185,250],> 250	-
Photon+Lepton Category		
Kinematic Cuts	Search Bins (GeV)	Vetoed Events
$p_{\mathrm{T}}^{\gamma} > 35$ GeV, $p_{\mathrm{T}}^{\mathrm{miss}} > 120$ GeV $p_{\mathrm{T}}^{\ell} > 25$ GeV, $M_T\left(\ell, p_{\mathrm{T}}^{\mathrm{miss}}\right) > 100$ GeV	$p_{\mathrm{T}}^{\mathrm{miss}}$: [120, 200], [200, 400], > 400 H_T: [0,100], [100, 400], > 400, p_{T}^{γ}: [35,200], > 200	-
Photon+S_T^{γ} Category		
Kinematic Cuts	Search Bins (GeV)	Vetoed Events
$p_{\mathrm{T}}^{\gamma} > 180$ GeV, $p_{\mathrm{T}}^{\mathrm{miss}} > 300$ GeV $S_T^{\gamma} > 600$ GeV, $M_T\left(\gamma, p_{\mathrm{T}}^{\mathrm{miss}}\right) > 300$ GeV	S_T^{γ}: [600, 800],[800, 1000] [1000,1300], > 1300	$H_T^{\gamma} > 2$ TeV if $p_{\mathrm{T}}^{\mathrm{miss}} > 350$ GeV Diphoton, Lepton
Photon+H_T^{γ} Category		
Kinematic Cuts	Search Bins (GeV)	Vetoed Events
$p_{\mathrm{T}}^{\gamma} > 100$ GeV, $p_{\mathrm{T}}^{\mathrm{miss}} > 350$ GeV $H_T^{\gamma} > 700$ GeV, $\lvert\Delta\phi\left(\pm\vec{p}_T^{miss}, \vec{p}_T^{\gamma}\right)\rvert > 0.3$	$p_{\mathrm{T}}^{\mathrm{miss}}$: [350,450], [450, 600], > 600 H_T^{γ}: [700, 2000], > 2000	$H_T^{\gamma} < 2$ TeV Diphoton, Lepton

Table 2: Predicted background yields and observed data for the Photon+S_T^{γ} category (left) and the Photon+H_T^{γ} category (right). The excess in the second bin of the Photon+H_T^{γ} category was also found in the initial search [16].

S_T^{γ} (GeV)	Total bkg.	Data
600 - 800	260.5 ± 29.6	273
800 - 1000	96.2 ± 13.9	98
1000 - 1300	50 ± 7.9	59
> 1300	16.8 ± 3.8	20

$p_{\mathrm{T}}^{\mathrm{miss}}$ (GeV)	Total bkg.	Data
350 - 450	5.7 ± 2.6	4
450 - 600	2.7 ± 0.9	10
> 600	2.5 ± 1	4

categories showing deviations from expectations. These deviations are not caused by changes applied in the combination with respect to the initial analysis.

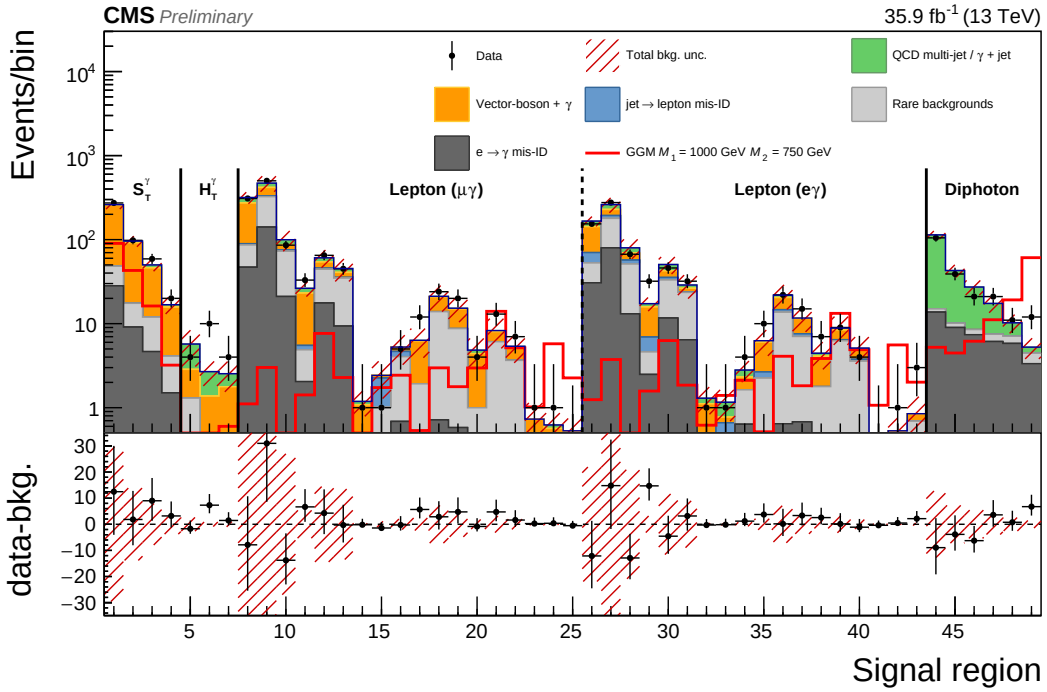

Figure 3: Comparison between the observed yield and the background prediction for all search bins used in the combination. The yields for the Photon+Lepton and Diphoton categories correspond to the published results, while the yields of the Photon+S_T^γ and Photon+H_T^γ categories are based on the modified event selections ensuring exclusive signal regions.

The results of the combination are interpreted in terms of the GGM scenario and simplified models introduced in Section 2. The 95% confidence level (CL) upper limits on the SUSY cross sections are calculated with the CL_s criterion [46, 47] using the LHC-style profile likelihood ratio as test statistic [48] evaluated in the asymptotic approximation [49]. Log-normal nuisance parameters are used to describe the systematic uncertainties, which follow the treatment used in the initial searches. The majority of the systematic uncertainties in the background predictions are not correlated between the four categories. Only the systematic uncertainties regarding the rare background predictions as well as the uncertainties assigned to the photon identification efficiency are treated as fully correlated between all four categories. In addition, uncertainties in the prediction of vector boson production in association with photons in the Photon+S_T^γ and Photon+Lepton categories are treated as fully correlated, since similar prediction methods are used. Furthermore, all systematic uncertainties affecting the signal acceptance are assumed to be fully correlated between the four categories.

Results for the GGM scenario are presented in the parameters that are scanned (M_1 and M_2) and in terms of physical mass parameters for the chargino and neutralino. Figure 4 (left) shows the combined expected exclusion limits for the M1M2 scenario, where the combination excludes almost all signal points up to $M_2 = 1300\,\text{GeV}$ across the full range of M_1. The figure indicates which category is able to exclude a particular signal point. The gray areas labeled as "combination" show the phase space where only the combination of the categories is expected to exclude the signal points. The area at large M_1 values, which is only covered by the Photon+Lepton category, corresponds to signal points with a wino-like NLSP reducing the

probability of a second high-energy photon in the event. Figure 4 (right) shows the observed and expected exclusion as a function of the physical masses of the lightest chargino and the lightest neutralino. The limits of the Diphoton and Photon+Lepton categories are nearly independent of the neutralino mass since these categories are inclusive in $p_{\mathrm{T}}^{\mathrm{miss}}$. The higher $p_{\mathrm{T}}^{\mathrm{miss}}$ regions used in the Photon+S_T^{γ} and Photon+H_T^{γ} categories mainly contribute closer to the mass diagonal at higher neutralino masses. The combination exceeds the sensitivity of the individual searches by around 100 GeV with respect to the wino mass parameter M_2, which translates to a gain of up to 100 GeV for the lower chargino mass limit. For low neutralino masses, the combination is able to improve the observed limit by up to 30 GeV. For higher neutralino masses, the combination does not improve on the current best observed limit mainly due to the discrepancy between data and expectation observed in the Diphoton category, which corresponds to an observed significance of the order of two standard deviations.

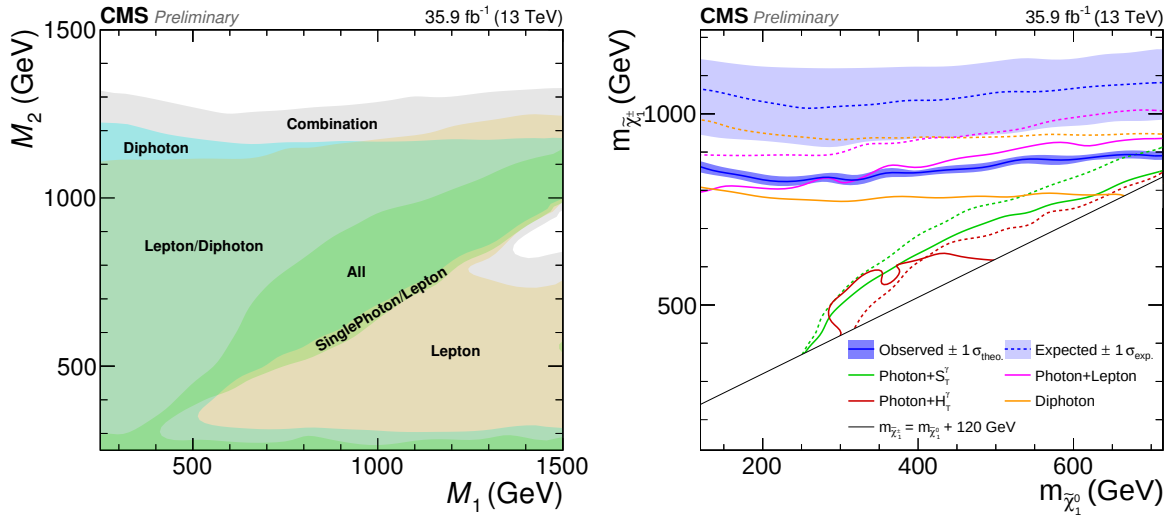

Figure 4: Combined exclusion limits for the M1M2 scenario in terms of the GGM model parameters (left) and the physical neutralino and chargino masses (right). The left panel shows the expected exclusion, while the right panel shows both the observed and the expected exclusion limits. In the physical mass plane only signal points with a mass splitting above 120 GeV are shown to enable a precise assignment of the physical masses and the GGM model parameters. The uncertainty bands around the expected and observed limit of the combination in the right panel correspond to the experimental ($\sigma_{\mathrm{exp.}}$) and theory uncertainty ($\sigma_{\mathrm{theo.}}$), respectively.

Figure 5 shows the combined NLSP mass exclusion for simplified topologies in electroweak scenarios varying the branching fraction of the neutralino (left) and chargino (right) decay. Here, the Photon+S_T^{γ} category provides the highest sensitivity along with the Diphoton category. Smaller contributions arise from the Photon+Lepton category. The sensitivity of the Photon+Lepton category to scenarios with large branching fractions of the decay $\tilde{\chi}_1^0 \to \gamma + \widetilde{G}$ especially arises from events where one photon is misidentified as lepton. For the Neutralino BF scenario, which probes $\tilde{\chi}_1^{\pm}\tilde{\chi}_1^0$ and $\tilde{\chi}_1^{\pm}\tilde{\chi}_1^{\mp}$ production, the combined exclusion for NLSP masses ranges from 1200 GeV for a branching fraction of 100% for the decay $\tilde{\chi}_1^0 \to \gamma + \widetilde{G}$ to 1000 GeV for 50%. For smaller branching fractions the sensitivity drops for all categories since the probability of a final state with at least one photon decreases. This combined exclusion almost coincides with the exclusion based on the Photon+S_T^{γ} category. In case of the Chargino BF scenario only $\tilde{\chi}_1^{\pm}\tilde{\chi}_1^{\mp}$ production is probed, leading to a smaller signal cross section. Here, an expected limit on the NLSP mass of up to 1000 GeV can be achieved for high branching fractions for the decay $\tilde{\chi}_1^{\pm} \to \tilde{\chi}_1^0(\gamma\widetilde{G}) + soft$. The largest gain in sensitivity from the combination is found at

a branching fraction of 40%, where the sensitivity of Photon+S_T^γ, Photon+Lepton, and Diphoton categories is of the same order. Observed gaugino mass limits are set up to 1000 GeV and 825 GeV in the Neutralino and the Chargino BF scenario, respectively.

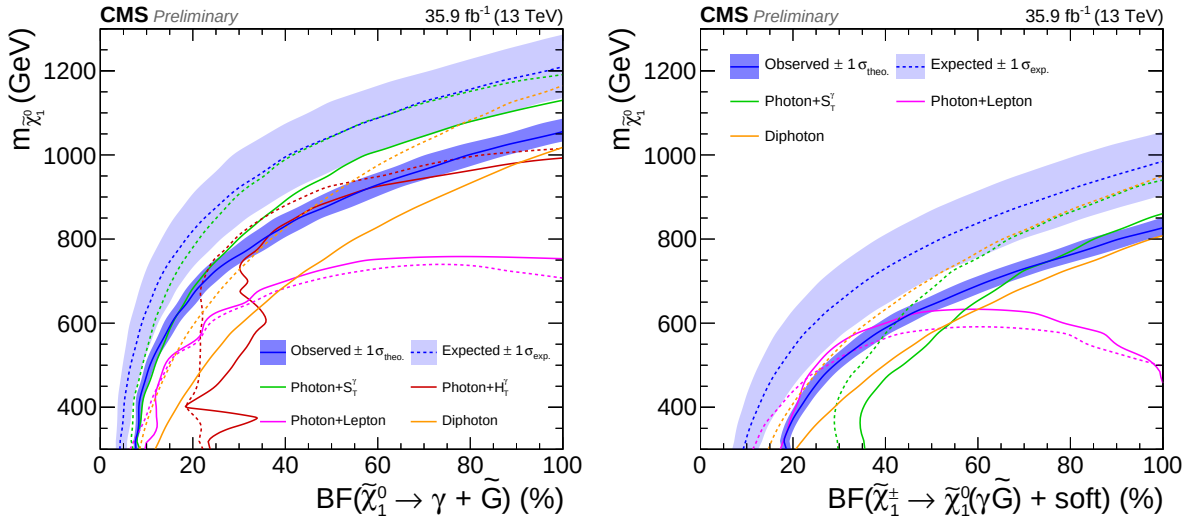

Figure 5: Combined exclusion for the Neutralino BF scenario (left), which probes $\tilde{\chi}_1^\pm\tilde{\chi}_1^0$ and $\tilde{\chi}_1^\pm\tilde{\chi}_1^\mp$ production combined with the NLSP BF scanned between decays to $Z\tilde{G}$ and $\gamma\tilde{G}$. Combined exclusion for the Chargino BF scenario (right), which probes $\tilde{\chi}_1^\pm\tilde{\chi}_1^\mp$ production combined with the Chargino BF scanned between decays to $W\tilde{G}$ and $\tilde{\chi}_1^0$ + soft, where the $\tilde{\chi}_1^0$ decays into a photon and a gravitino. The uncertainty bands around the expected and observed limit of the combination correspond to the experimental ($\sigma_{\text{exp.}}$) and theory uncertainty ($\sigma_{\text{theo.}}$), respectively.

The results from simplified topologies in strong /gluino production scenarios are shown in Fig. 6. For these topologies the Diphoton category is not included in the combination, which allows for a removal of the diphoton veto discussed in Section 5 and mainly increases the sensitivity of the Photon+H_T^γ category. In case of the nominal Gluino scenario, introduced in Section 2, the combination shows an optimal expected exclusion compared to the different individual categories across the widest region of the mass parameter space. For NLSP masses below 1000 GeV the sensitivity of the combination is dominated by the Photon+H_T^γ category, which mainly targets signal events with large hadronic activity. However, at NLSP masses above 1700 GeV the Photon+S_T^γ category, which benefits from the smaller hadronic activity close to the mass diagonal, provides the highest sensitivity. The Photon+Lepton category selects events where the W decays leptonically leading to a reduced sensitivity compared to the inclusive categories. The largest improvement of the combination is achieved in the phase space where the sensitivity of both inclusive categories is of the same order. Here, the expected limit on the gluino mass can be improved by 50 GeV. The right plot of Fig. 6 shows the same SMS topology for a fixed gluino mass of 1950 GeV but varying the gluino branching fraction ratio between its charged and uncharged decay. A similar behavior compared to the nominal Gluino scenario with respect to the sensitivity of the two inclusive categories is found.

In most of the simplified topologies, the combination of the different categories outperforms the individual searches with respect to the expected limit. The right plot of Fig. 6 shows slight degradation at medium branching fractions for the combination compared to the Photon+H_T^γ category. This is due to the removal of the events with moderate H_T^γ and lepton events from the Photon+H_T^γ category as explained in Section 5. This strategy is motivated by optimizing the sensitivity to the GGM scenario shown in Fig. 4. In terms of the observed limits only small to no improvements compared to the individual searches can be found in all interpretations.

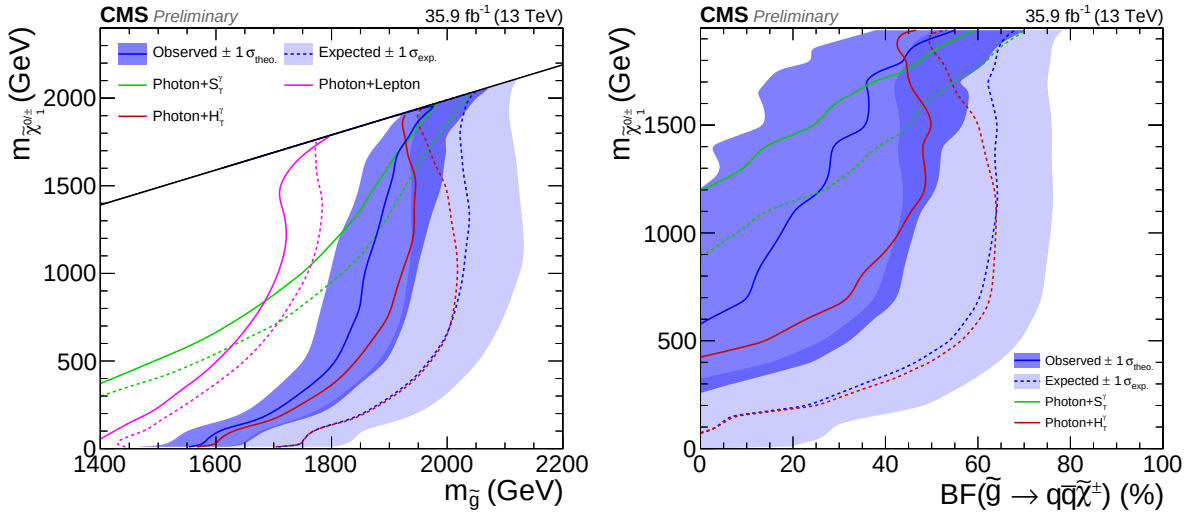

Figure 6: Combined exclusion for the nominal Gluino scenario (left) assuming equal probabilities for the charged and uncharged gluino decay. For the Gluino BF scenario (right) the ratio of the probabilities for both decays are scanned and the gluino mass is fixed to 1950 GeV. For both interpretations the Diphoton category is not used. The uncertainty bands around the expected and observed limit of the combination correspond to the experimental ($\sigma_{\text{exp.}}$) and theory uncertainty ($\sigma_{\text{theo.}}$), respectively.

This is mainly caused by an excess found in the Diphoton category [19], which provides the highest sensitivity across a wide range of phase spaces. Furthermore, also in each of the three remaining searches smaller excesses in data with respect to the background prediction and thus slight discrepancies between observed and expected limit are found. Combining the individual searches increases this effect resulting in a larger difference between the observed and expected exclusions.

7 Summary

A combination of four different searches for gauge-mediated supersymmetry in final states with photons and a large transverse momentum imbalance has been performed. Based on the event selection of the individual searches four event categories were defined. Overlaps between the categories were removed by additional vetoes designed to maximize the sensitivity of the combination. Using 36 fb^{-1} of data recorded by the CMS detector at the LHC at a center-of-mass energy of 13 TeV the combination maximizes the exclusion power of the searches described in [16–19].

The results are interpreted in the context of General Gauge Mediation (GGM) and in model-independent mass scans using simplified topologies. The sensitivity of the combination is also interpreted across a range of branching fractions allowing for generalization to a wide range of SUSY scenarios. The GGM scan is performed in an M_1 and M_2 parameter space where most of the signal points below $M2 < 1100$ (1300) GeV are excluded based on the observed (expected) limit. The results of the GGM scenario is also shown in physical mass parameters, which show competitive constraints on the chargino and neutralino masses. Here, chargino masses up to 890 (1080) GeV are excluded by the the observed (expected) limit across the tested neutralino mass spectrum. For a strong production scenario based on gluino pair production the highest observed (expected) excluded gluino masses are at 1975 (2050) GeV. In electroweak production models observed (expected) limits for neutralino masses are set up to

1050 (1200) GeV for combined $\widetilde{\chi}_1^{\pm}\widetilde{\chi}_1^0$ and $\widetilde{\chi}_1^{\pm}\widetilde{\chi}_1^{\mp}$ production, while for pure $\widetilde{\chi}_1^{\pm}\widetilde{\chi}_1^{\mp}$ production these limits are reduced to 850 (1000) GeV. The combination improves on the expected limits on neutralino and chargino masses by 100 GeV while the expected limit on the gluino mass is increased by 50 GeV compared to the individual searches.

References

[1] M. Dine and W. Fischler, "A phenomenological model of particle physics based on supersymmetry", *Phys. Lett. B* **110** (1982) 227, doi:10.1016/0370-2693(82)91241-2.

[2] L. Alvarez-Gaume, M. Claudson, and M. B. Wise, "Low-energy supersymmetry", *Nucl. Phys. B* **207** (1982) 96, doi:10.1016/0550-3213(82)90138-9.

[3] C. R. Nappi and B. A. Ovrut, "Supersymmetric extension of the SU(3)xSU(2)xU(1) model", *Phys. Lett. B* **113** (1982) 175, doi:10.1016/0370-2693(82)90418-X.

[4] M. Dine and A. E. Nelson, "Dynamical supersymmetry breaking at low energies", *Phys. Rev. D* **48** (1993) 1277, doi:10.1103/PhysRevD.48.1277, arXiv:hep-ph/9303230.

[5] M. Dine, A. E. Nelson, and Y. Shirman, "Low energy dynamical supersymmetry breaking simplified", *Phys. Rev. D* **51** (1995) 1362, doi:10.1103/PhysRevD.51.1362, arXiv:hep-ph/9408384.

[6] M. Dine, A. E. Nelson, Y. Nir, and Y. Shirman, "New tools for low-energy dynamical supersymmetry breaking", *Phys. Rev. D* **53** (1996) 2658, doi:10.1103/PhysRevD.53.2658, arXiv:hep-ph/9507378.

[7] G. R. Farrar and P. Fayet, "Phenomenology of the production, decay, and detection of new hadronic states associated with supersymmetry", *Phys. Lett. B* **76** (1978) 575, doi:10.1016/0370-2693(78)90858-4.

[8] S. Dimopoulos, G. F. Giudice, and A. Pomarol, "Dark matter in theories of gauge mediated supersymmetry breaking", *Phys. Lett. B* **389** (1996) 37, doi:10.1016/S0370-2693(96)01241-5, arXiv:hep-ph/9607225.

[9] S. P. Martin, "Generalized messengers of supersymmetry breaking and the sparticle mass spectrum", *Phys. Rev. D* **55** (1997) 3177, doi:10.1103/PhysRevD.55.3177, arXiv:hep-ph/9608224.

[10] E. Poppitz and S. P. Trivedi, "Some remarks on gauge mediated supersymmetry breaking", *Phys. Lett. B* **401** (1997) 38, doi:10.1016/S0370-2693(97)00367-5, arXiv:hep-ph/9703246.

[11] P. Meade, N. Seiberg, and D. Shih, "General Gauge Mediation", *Prog. Theor. Phys. Suppl.* **177** (2009) 143–158, doi:10.1143/PTPS.177.143, arXiv:0801.3278.

[12] M. Buican, P. Meade, N. Seiberg, and D. Shih, "Exploring general gauge mediation", *JHEP* **03** (2009) 016, doi:10.1088/1126-6708/2009/03/016, arXiv:0812.3668.

[13] S. Abel, M. J. Dolan, J. Jaeckel, and V. V. Khoze, "Phenomenology of pure general gauge mediation", *JHEP* **12** (2009) 001, doi:10.1088/1126-6708/2009/12/001, arXiv:0910.2674.

[14] L. M. Carpenter, M. Dine, G. Festuccia, and J. D. Mason, "Implementing general gauge mediation", *Phys. Rev. D* **79** (2009) 035002, doi:10.1103/PhysRevD.79.035002, arXiv:0805.2944.

[15] T. T. Dumitrescu, Z. Komargodski, N. Seiberg, and D. Shih, "General Messenger Gauge Mediation", *JHEP* **05** (2010) 096, doi:10.1007/JHEP05(2010)096, arXiv:1003.2661.

[16] CMS Collaboration, "Search for supersymmetry in events with at least one photon, missing transverse momentum, and large transverse event activity in proton-proton collisions at $\sqrt{s} = 13$ TeV", *JHEP* **12** (2017) 142, doi:10.1007/JHEP12(2017)142, arXiv:1707.06193.

[17] CMS Collaboration, "Search for gauge-mediated supersymmetry in events with at least one photon and missing transverse momentum in pp collisions at $\sqrt{s} = 13$ TeV", *Phys. Lett.* **B780** (2018) 118–143, doi:10.1016/j.physletb.2018.02.045, arXiv:1711.08008.

[18] CMS Collaboration, "Search for supersymmetry in events with a photon, a lepton, and missing transverse momentum in proton-proton collisions at $\sqrt{s} = 13$ TeV", *JHEP* **01** (2019) 154, doi:10.1007/JHEP01(2019)154, arXiv:1812.04066.

[19] CMS Collaboration, "Search for supersymmetry in final states with photons and missing transverse momentum in proton-proton collisions at 13 TeV", (2019). arXiv:1903.07070. Submitted to JHEP.

[20] CMS Collaboration, "Interpretation of searches for supersymmetry with simplified models", *Phys. Rev. D* **88** (2013) 052017, doi:10.1103/PhysRevD.88.052017, arXiv:1301.2175.

[21] P. Grajek, A. Mariotti, and D. Redigolo, "Phenomenology of General Gauge Mediation in light of a 125 GeV Higgs", *JHEP* **07** (2013) 109, doi:10.1007/JHEP07(2013)109, arXiv:1303.0870.

[22] S. Knapen, D. Redigolo, and D. Shih, "General Gauge Mediation at the Weak Scale", *JHEP* **03** (2016) 046, doi:10.1007/JHEP03(2016)046, arXiv:1507.04364.

[23] S. Knapen and D. Redigolo, "Gauge mediation at the LHC: status and prospects", *JHEP* **01** (2017) 135, doi:10.1007/JHEP01(2017)135, arXiv:1606.07501.

[24] W. Beenakker, R. Hopker, and M. Spira, "PROSPINO: A Program for the production of supersymmetric particles in next-to-leading order QCD", arXiv:hep-ph/9611232.

[25] A. Buckley et al., "LHAPDF6: parton density access in the LHC precision era", *Eur. Phys. J.* **C75** (2015) 132, doi:10.1140/epjc/s10052-015-3318-8, arXiv:1412.7420.

[26] J. Butterworth et al., "PDF4LHC recommendations for LHC Run II", *J. Phys.* **G43** (2016) 023001, doi:10.1088/0954-3899/43/2/023001, arXiv:1510.03865.

[27] NNPDF Collaboration, "Parton distributions for the LHC Run II", *JHEP* **04** (2015) 040, doi:10.1007/JHEP04(2015)040, arXiv:1410.8849.

[28] The NNPDF collaboration et al., "Parton distributions for the lhc run ii", *Journal of High Energy Physics* **2015** (Apr, 2015) 40.

[29] CMS Collaboration, "Event generator tunes obtained from underlying event and multiparton scattering measurements", *Eur. Phys. J.* **C76** (2016), no. 3, 155, doi:10.1140/epjc/s10052-016-3988-x, arXiv:1512.00815.

[30] W. Beenakker et al., "Production of Charginos, Neutralinos, and Sleptons at Hadron Colliders", *Phys. Rev. Lett.* **83** (1999) 3780, doi:10.1103/PhysRevLett.83.3780, arXiv:hep-ph/9906298. [Erratum: *Phys. Rev. Lett.* **100** (2008) 029901, doi:10.1103/PhysRevLett.100.029901].

[31] B. Fuks, M. Klasen, D. R. Lamprea, and M. Rothering, "Gaugino production in proton-proton collisions at a center-of-mass energy of 8 TeV", *JHEP* **10** (2012) 081, doi:10.1007/JHEP10(2012)081, arXiv:1207.2159.

[32] B. Fuks, M. Klasen, D. R. Lamprea, and M. Rothering, "Precision predictions for electroweak superpartner production at hadron colliders with RESUMMINO", *Eur. Phys. J. C* **73** (2013) 2480, doi:10.1140/epjc/s10052-013-2480-0, arXiv:1304.0790.

[33] W. Beenakker, R. Hopker, M. Spira, and P. M. Zerwas, "Squark and gluino production at hadron colliders", *Nucl. Phys. B* **492** (1997) 51, doi:10.1016/S0550-3213(97)80027-2, arXiv:hep-ph/9610490.

[34] A. Kulesza and L. Motyka, "Threshold resummation for squark-antisquark and gluino-pair production at the LHC", *Phys. Rev. Lett.* **102** (2009) 111802, doi:10.1103/PhysRevLett.102.111802, arXiv:0807.2405.

[35] A. Kulesza and L. Motyka, "Soft gluon resummation for the production of gluino-gluino and squark-antisquark pairs at the LHC", *Phys. Rev. D* **80** (2009) 095004, doi:10.1103/PhysRevD.80.095004, arXiv:0905.4749.

[36] W. Beenakker et al., "Soft-gluon resummation for squark and gluino hadroproduction", *JHEP* **12** (2009) 041, doi:10.1088/1126-6708/2009/12/041, arXiv:0909.4418.

[37] W. Beenakker et al., "Squark and Gluino Hadroproduction", *Int. J. Mod. Phys. A* **26** (2011) 2637, doi:10.1142/S0217751X11053560, arXiv:1105.1110.

[38] C. Borschensky et al., "Squark and gluino production cross sections in pp collisions at $\sqrt{s}$ = 13, 14, 33 and 100 TeV", *Eur. Phys. J. C* **74** (2014) 3174, doi:10.1140/epjc/s10052-014-3174-y, arXiv:1407.5066.

[39] S. Abdullin et al., "The fast simulation of the CMS detector at LHC", *J. Phys.: Conf. Ser.* **331** (2011) 032049, doi:10.1088/1742-6596/331/3/032049.

[40] CMS Collaboration, "Performance of photon reconstruction and identification with the CMS detector in proton-proton collisions at $\sqrt{s} = 8$ TeV", *JINST* **10** (2015) P08010, doi:10.1088/1748-0221/10/08/P08010, arXiv:1502.02702.

[41] CMS Collaboration, "The CMS experiment at the CERN LHC", *JINST* **3** (2008) S08004, doi:10.1088/1748-0221/3/08/S08004.

[42] CMS Collaboration, "Particle-flow reconstruction and global event description with the CMS detector", *JINST* **12** (2017), no. 10, P10003, doi:10.1088/1748-0221/12/10/P10003, arXiv:1706.04965.

[43] M. Cacciari, G. P. Salam, and G. Soyez, "The anti-k_t jet clustering algorithm", *JHEP* **04** (2008) 063, doi:10.1088/1126-6708/2008/04/063, arXiv:0802.1189.

[44] CMS Collaboration, "Performance of missing transverse momentum in pp collisions at sqrt(s)=13 TeV using the CMS detector", CMS Physics Analysis Summary CMS-PAS-JME-17-001, 2018.

[45] K. Rehermann and B. Tweedie, "Efficient Identification of Boosted Semileptonic Top Quarks at the LHC", *JHEP* **03** (2011) 059, doi:10.1007/JHEP03(2011)059, arXiv:1007.2221.

[46] T. Junk, "Confidence level computation for combining searches with small statistics", *Nucl. Instrum. Meth. A* **434** (1999) 435, doi:10.1016/S0168-9002(99)00498-2, arXiv:hep-ex/9902006.

[47] A. L. Read, "Presentation of search results: the CLs technique", *J. Phys. G* **28** (2002) 2693, doi:10.1088/0954-3899/28/10/313.

[48] ATLAS, CMS, and LHC Higgs Combination Group collaborations, "Procedure for the LHC Higgs boson search combination in Summer 2011", Technical Report CMS-NOTE-2011-005. ATL-PHYS-PUB-2011-11, 2011.

[49] G. Cowan, K. Cranmer, E. Gross, and O. Vitells, "Asymptotic formulae for likelihood-based tests of new physics", *Eur. Phys. J. C* **71** (2011) 1554, doi:10.1140/epjc/s10052-011-1554-0, arXiv:1007.1727. [Erratum: doi:10.1140/epjc/s10052-013-2501-z].